MODELLING INTERGRANULAR CRACK PROPAGATION TO AID MICROSTRUCTURE ENGINEERING. PART I: MODELS

A. Jivkov[1]

Keywords: intergranular cracking, stainless steels, microstructure, Grain boundaries, crack bridging, finite element analysis

MSC 2000: 74R10

ABSTRACT

A comprehensive account of new 2D and 3D mechanical models for studying intergranular environment assisted crack propagation in polycrystalline materials is presented in this first part of the work. The models are developed to eliminate the limitations of the percolation models, used previously to assess resistance of materials to intergranular cracking. The percolation models do not account for the mechanical crack driving force, which limits their applicability. The new models are based on a regular discrete representation of the microstructure of the materials and a binary selection of grain boundaries' properties, where the grain boundaries are assumed to be either resistant or susceptible to cracking depending on the grain boundary character. The problems solved and methods of analysis of the results presented in the second part of the work are also described.

1. Introduction

Cracks in polycrystalline materials may propagate along the boundaries between the grains or crystals (intergranular cracking), through the grains (transgranular cracking), or in a combined manner (mixed-mode cracking) [1]. A crack for which the mechanical crack driving force alone is not sufficient to trigger crack propagation is called sub-critical or short. Such a crack would not be predicted to propagate using classical fracture mechanics methodology. However, it could still advance as a result of some environment stimulated physical process, such as corrosion or diffusion of embrittling species. In many situations

---
[1] Andrey Jivkov, The University of Manchester, School of Materials, Grosvenor Street, Manchester M1 7HS, UK; Tel: +44 (0)161 3063556; Fax: +44 (0)161 3063586; E-mail: andrey.jivkov@manchester.ac.uk

grain boundaries are sites of preferential environment attack and the intergranular cracking mode dominates the sub-critical propagation stage [2]. This process is generically referred to as intergranular environment assisted cracking (IGEAC). It is observed to happen in susceptible stainless alloys, such as nickel-based alloys and austenitic stainless steels used in structural components in the power generation industry [3]. The lifetime of such components is difficult to assess because of uncertainties in short crack behaviour. One source of uncertainty is the material microstructure, which may be described with the sizes and distribution of the grains, and the types and connectivity of the grain boundaries. Attention in this work is given to the role played by grain boundary types. The notion of grain boundary type or character is related to the energy of the grain boundary. Grain boundaries have internal energies larger than the internal energy of the ideal crystal but smaller than the material free surface energy. The excess of energy compared to the ideal crystal is due to the mismatch between the atomic layers of the two grains adjacent to the boundary. According to the coincidence site lattice (CSL) model [4], grain boundaries are classified by the degree of lattice coincidence, i.e. the area density of interface atoms that are common for both crystals. The character, Σ, of the grain boundary is reciprocal of this density, so that boundaries of high degree of coincidence have low Σ and low internal energy, and boundaries with low degree of coincidence (or no special crystallographic relationship) have high Σ and high internal energy. The low Σ boundaries are called "special" and the high Σ boundaries are called "random". Experimental results, e.g. [5, 6] for nickel based alloys and [7, 8] for sensitised stainless steels, show that random grain boundaries are more prone to intergranular corrosion and stress corrosion than special grain boundaries. Random boundaries form paths of low resistance for intergranular corrosion and stress corrosion cracking, while increasing the fraction of special grain boundaries has been shown to improve resistance to corrosion and cracking. Grain boundary engineering (GBE) is a generic term for thermo-mechanical treatment techniques that have a primary goal to improve the microstructure resistance to intergranular damage by increasing the fraction of special boundaries and disrupting the connectivity of random boundaries [9]. In view of the possibilities GBE offers, it is essential to have models that can estimate the overall resistance of microstructures of various properties.

A first simplification to modelling a microstructure is to classify the grain boundaries into two categories – "resistant" and "susceptible" to intergranular corrosion and cracking. These correspond to the special and the random boundaries according to the CSL classification, respectively. This is a useful assumption for fully sensitised stainless steels, in which the grain boundary structure controls the degree of carbide precipitation [10]. This locally reduces the grain boundary chromium content, and thus lowers its corrosion resistance. In other intergranular corrosion systems, and partial sensitisation of stainless steels, a spectrum of boundary properties develops, but this issue is outside the scope of the present work. The binary classification of grain boundaries allows for a percolation approach in studying the overall resistance of a microstructure to IGEAC and in estimating the impact of grain boundary engineering. The essence of the percolation approach is that a crack approaching a triple junction (the meeting point of three grain boundaries) along one boundary is either allowed to propagate or forced to arrest depending on the characters of the remaining two boundaries. The purpose of percolation simulations would be to determine the size of the susceptible boundary paths for a given microstructure and the threshold fraction of resistant boundaries required to interrupt the percolating network. Before proceeding with the percolation approach, a second typical simplification is to adopt a regular geometrical representation of the microstructure. Regular 2D models can choose either a square or hexagonal cell structure, where a cell substitutes one grain. A higher coordination number in

hexagonal meshes is better, so this has been the standard unit cell in the previously proposed 2D percolation-like models, e.g. [11, 12]. For the hexagonal cell structure, the critical fraction of resistant boundaries, i.e. the percolation threshold, is mathematically found to be around 0.65 [13]. Regular 3D models can choose from more shapes, such as cubes with 6 square faces, rhombic dodecahedra with 12 identical rhombic faces, and truncated octahedra with 6 square and 8 regular hexagonal faces. The truncated octahedron, also called tetrakaidecahedron or mecon, offers the best coordination number 14 and has been used in 3D percolation-like models [14, 15]. The percolation threshold for the meconal structure was found to be around 0.23 [13].

While the percolation-like models have been successful in assessing the probable extent of crack growth, a common drawback for all of them is that they do not account for the mechanical component of IGEAC, namely the crack driving force, which can vary during crack evolution. It ought to be mentioned that some of the percolation-like models consider the grain boundary orientation with respect to the applied load in the decision for further percolation, but the account for the mechanical component is limited to this. The true development of the crack driving force is clearly of importance. For example, crack branching, observed experimentally [8] and in model simulations [13], would reduce the driving force for the main crack. Further, experimental studies have shown that the interaction between the crack and resistant grain boundaries leads to crack bridging [16, 17]. The bridges are formed when the propagating crack deviates around resistant boundaries. Thus the bridging ligaments are left behind the crack front and a mechanical crack shielding effect from these is expected to reduce the crack tip strains and thereby retard crack propagation, particularly for short cracks. In order to study these microstructure effects on the materials resistance to IGSCC, mechanical finite element based models have been recently developed. These models follow the assumptions of the percolation-like models using hexagonal microstructures in 2D [18] and meconal microstructures in 3D [19] and a binary classification of grain boundaries. The two parts of this work present a description of the models and a selection of the results obtained to date. The selection aims at demonstrating the significant impact of the mechanical load, branching and bridging on the developed crack lengths and critical thresholds of resistant boundary fractions when compared to percolation-like models predictions. Further, the impact of the failure properties of susceptible and resistant boundaries is shown. It should be mentioned that the models presented do not account for the kinetics of crack propagation and should be viewed as an advance from the percolation-like models by including mechanical effects. In this sense the models are tools for assessing the relative microstructure resistance to intergranular fracture. Applied to IGSCC, the models are relevant only to fully sensitised materials, similarly to percolation-like models. The new models, however, allow for the incorporation of the dependence of propagation kinetics on local mechanical fields, which is a topic of ongoing work [20].

2. Microstructure Models

2.1. Physical Description

A region of a polycrystalline material is an assembly of grains. As a first approximation this assembly is represented by a regular tessellation of space into identical cells, where each cell corresponds to one material grain. The cell diameter corresponds to the average grain size in the real material. Grains are assumed to be represented by regular hexagons in 2D and truncated octahedrons in 3D, see Fig.1. Firstly, these two shapes are

capable of filling their respective spaces compactly. Secondly, among the space filling shapes in their respective spaces, these two shapes have coordination numbers (number of neighbouring grains) closest to those observed in reality. A major geometry parameter is the unit cell diameter, D. This is the diameter of the circumscribing circle for 2D cells and the edge of the cell bounding cube for 3D cells. The model material is a Type 304 austenitic stainless steel, with typical values for Young's modulus $E = 193$ GPa, Poisson's ratio $\nu = 0.29$, proof stress (at 0.2% plastic strain) $\sigma_0 = 310$ MPa, and tensile strength (at 60% elongation) $\sigma_u = 600$ MPa. These are taken as the homogeneous mechanical properties of the model, i.e. when the assembly is considered as a continuum, and are used in constructing the computational model described in the next subsection. The yield strain $\varepsilon_0 = \sigma_0 / E$ is defined for future reference.
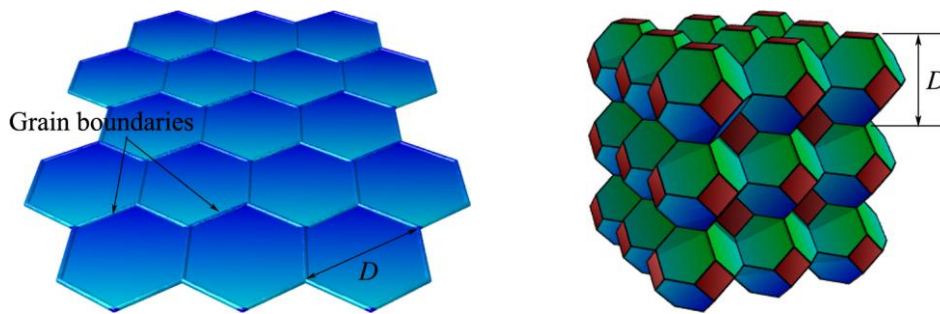

Figure 1. Regions of 2D (hexagonal) and 3D (meconal) model microstructures

Grain boundaries (the common faces in the assembly of cells) are assumed to belong to either of two classes. The first class consisfs of special (low-angle, low-energy) grain boundaries, which are generally accepted to be resistant to corrosion. The second class includes random (high-angle, high-energy) grain boundaries, which are found to be susceptible to corrosion. The fraction of resistant boundaries, f, defined as the number of resistant divided by the total number of boundaries is a major parameter in the current studies. The distribution of resistant boundaries in the assembly is randomly assigned for given f.

Cracks are assumed to propagate along grain boundaries only. In the model presented here, the kinetics of the stress corrosion mechanism are not accounted for, so the real time dimension of crack propagation is not determined and crack velocities are not calculated. Experimental observations of intergranular stress corrosion show that susceptible boundaries fail at crack opening displacements of the order of several nano-meters with insignificant plastic deformations [8, 21]. This suggests that the failure strain of susceptible boundaries, denoted by ε_{sf}, is around or below the apparent material yield strain, ε_0. The failure strain ε_{sf} is a second model parameter. Resistant boundaries, in contrast to susceptible boundaries, can yield and rupture well into the plastic region, as demonstrated by in-situ high resolution tomographic and fractographic observations of intergranular stress corrosion cracking [16, 17]. Therefore, resistant boundaries in the model are also allowed to fail but after significant amount of accumulated plastic strain, denoted by ε_{rf} and defining a third model parameter. The resistant boundaries failure strain is assumed to be a multiple of the yield strain ε_0, but a fraction of the material elongation at rupture.

2.2. Computational Description

A direct approach to model an assembly of cells in a finite element environment would be based on continuum mechanics. Each cell would have to be tessellated into available shapes of continuum elements (triangles and quadrilaterals in 2D and tetrahedral, triangular prisms and parallelepipeds in 3D) and connected to the neighbouring cells with some interface elements, representing the grain boundaries. Such a direct modelling strategy requires an enormous amount of computer resources involved in the simulations, especially for 3D models. A discrete representation of the assembly is suggested instead [18, 19]. In the discrete model, each cell is represented as a geometrical point and its connections to the neighbouring cells, which are the grain boundaries in reality, are represented by structural members of linear extension. The idea is illustrated in Fig. 2, where a portion of a plane hexagonal mesh and its corresponding plane structure, and a cell of the meconal mesh and its corresponding space structure are shown. In both cases the finite element model consists of nodes, placed in the centres of the grains, and beam-type finite elements for structural members. Thus, the grains deformability is transferred to the deformability of the adjacent beam elements.
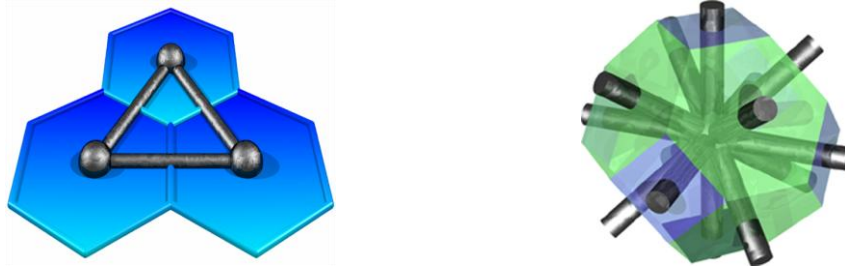

Figure 2. Discrete representation of 2D (hexagonal) and 3D (meconal) microstructures

The discrete representation leads to a significant reduction of the nodes and elements in a model and hence of the computational effort, which is crucial for three dimensional problems. Essential to the discrete model is the question of how well it represents solid behaviour. This question is connected to the selection of elements cross-section properties (section area and moments of inertia) and deformation properties (forces and moments versus relative displacements and rotations). Since regular geometry introduces preferential directions in the assembly, it is generally impossible to make a selection so that the discrete assembly behaves as a continuum solid for all modes of deformation simultaneously. It is possible, however, using a calibration procedure to make such a selection for every particular deformation mode. In the present work, selections of beam cross sections are made for both 2D and 3D, so that the assembly in question subject to tensile deformation in the elastic range behaves like a solid under the same deformation. This is viewed as a good first approximation, while the continuum approach is left for the future as more computational power becomes available. It should be further noted that in the course of crack propagation the beams representing susceptible boundaries would fail upon reaching their prescribed failure strain ε_{sf}, which is a fraction of the material yield strain ε_0, while the beams representing resistant boundaries would fail upon reaching their prescribed failure strain ε_{rf}, which is a multiple ε_0. The average strain, i.e. the strain in the centre of the cross section in beam elements is used in the calculations. Thus the beam elements in the computational model have dual service. They represent the deformability of the portions of the two neighbouring grains and obey the failure properties of the grain boundary they stand for.

133

3. Crack advance strategies

The strategy for crack advance in the computational model relies on a series of finite element solutions for equilibrium of the (evolving) assembly with the applied loads. Each solution provides the stresses and strains at the grain boundaries (midpoints of the beam elements), necessary to decide upon further crack propagation. If the failure strain of a grain boundary, being either resistant or susceptible, is reached, that boundary is a candidate for failure. In general, only one boundary, the most critical, is allowed to fail at a time, i.e. one beam element is deleted from the discrete structure. As every failure event leads to stresses and strains redistribution that cannot be judged in advance, the single-failure strategy insures that the recalculated equilibrium will deliver the correct stresses and strains. This strategy means that the applied load is thought of as decreased to a level where only one candidate for failure exists. Hence the mechanical equilibrium found by finite elements is physically unstable for an advancing crack and turns into physical equilibrium only for the arrested crack.

The search for boundaries that are candidates for failure determines two types of crack advance schemes. The first type is a "step" advance scheme used for crack propagation in 3D microstructures, where bridges formation is expected to occur naturally. The second type is a "jump" advance scheme used for crack propagation in 2D microstructures to allow for bridging mimicking 3D behaviour. These are explained below, assuming a crack grown to a certain stage and an equilibrium solution found for the corresponding discrete model.

3.1. "Step" advance scheme

The step crack advance is illustrated in Fig. 3 on a 2D geometry for clarity, but is applicable to the 3D case. The current crack is shown with thick white lines and all boundaries that are in contact with the crack surface are shown with thick red lines. These boundaries are in direct contact with (exposed to) the corrosive environment and the search for candidates for failure is performed only among them. Let ε_i is the strain in the i-th exposed boundary, calculated with the finite element solution for equilibrium of the current configuration. Let ε_{if} be the failure strain of this boundary, i.e. $\varepsilon_{if} = \varepsilon_{sf}$ if the boundary is susceptible and $\varepsilon_{if} = \varepsilon_{rf}$ if the boundary is resistant. All boundaries with $(\varepsilon_i - \varepsilon_{if}) > 0$ are candidates for failure at the current simulation step. If there are no such boundaries, the crack is arrested, the assembly is in equilibrium with the applied loads, and the simulation terminates. Otherwise, the boundary with maximum $(\varepsilon_i - \varepsilon_{if})$ is selected as critical, the corresponding beam element is removed from the structure, and the simulation continues.
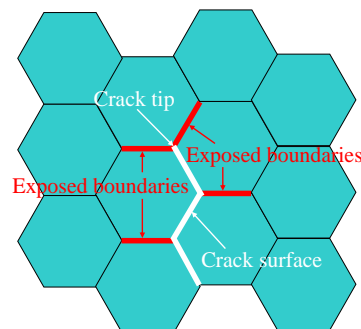

Figure 3. Search for failing boundaries according to the step advance scheme, applicable to 3D microstructures

3.2. "Jump" advance scheme

Fig. 4 illustrates the jump advance scheme. As in Fig. 3, the crack is shown with thick white lines. The exposed boundaries are shown with thick red lines and denoted by e. In addition, the next level (sub-exposed) boundaries which are in contact with exposed boundaries are shown with thick yellow lines and denoted by e'. Initially, this scheme follows the step advance scheme, forming (ε_i - ε_{if}) for each surface boundary. If there are exposed boundaries with (ε_i - ε_{if}) > 0 the boundary with maximum (ε_i - ε_{if}) is accepted as critical, the corresponding beam element is removed from the structure, and the simulation continues. If there are no such exposed boundaries, the sub-exposed boundaries are considered. The reason to consider sub-exposed boundaries is to mimic the real 3D behaviour. Consider, for example, the boundary between points A and B in Fig. 4. If this was resistant, this would prevent it from failing at the current simulation step. In the real 3D situation, the crack could pass from point A to point B via an out-of-plane path along susceptible boundaries. This places the sub-exposed boundaries adjacent to point B in contact with the environment, i.e. they become exposed boundaries. The same possibility for by-passing the current surface boundaries exists for all of the sub-exposed boundaries. Depending on the total crack geometry (not only the portion shown in the figure), the critical sub-exposed boundary could be either adjacent to point B, or adjacent to point C, or somewhere else. Therefore, if any of the exposed boundaries cannot fail at a given simulation step, all sub-exposed boundaries are reconsidered as exposed boundaries and the same strategy for failing holds. If there are no candidates for failure among the sub-exposed boundaries, the crack is assumed arrested and simulations are terminated.
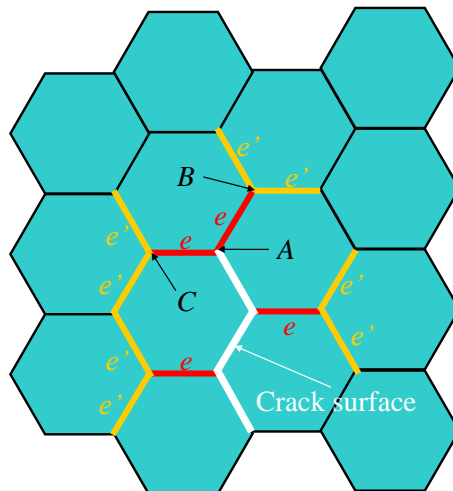

Figure 4. Search for failing boundaries according to the jump advance scheme, applicable to 2D microstructures

The crack advance schemes described above are implemented by an in-house computer programme. The programme is responsible for creating the initial model and consecutively calling external equilibrium solver, ABAQUS [22], deciding upon crack advance from the equilibrium solution and changing the model if required.

4. Problems description

4.1. 3D Geometry problems

Fig. 5 shows the 3D solid region that is modelled via tessellation into an assembly of mecons. With respect to a fixed coordinate system (X_1, X_2, X_3), the assembly fills the region $\{-7.5D \leq X_1 \leq 7.5D, -20D \leq X_2 \leq 20D, 0 \leq X_3 \leq 25D\}$. This region contains 30000 grains, which form 198310 internal grain boundaries, modelled by 30000 nodes and 198310 beam elements in the finite element model. A pre-crack, is assumed shown with a thick white segment on the surface $X_1 = 0$. The pre-crack is introduced by removing the three beam elements intersecting the plane rectangle given by $\{-0.5D \leq X_2 \leq 0.5D, 0 \leq X_3 \leq 0.5D\}$. This corresponds to an initial semi-circular crack of radius $0.5D$ placed at the origin of the coordinate system with surface perpendicular to the X_1 axis. In view of the applied load, the single crack is expected to grow predominantly parallel to the X_2 axis on the surface and parallel to the X_3 axis in depth. The load is applied via prescribed displacements: $u_1 = -0.00375D$ along the boundary plane $X_1 = -7.5D$ and $u_1 = 0.00375D$ along the boundary plane $X_1 = 7.5D$. Further, $u_3 = 0$ is prescribed along the boundary plane $X_3 = 25D$, while all other boundaries are stress free. These boundary conditions introduce a homogeneous strain in the assembly $\varepsilon_\infty = 5\mathrm{x}10^{-4}$, equivalent to a homogeneous stress $\sigma_\infty \approx 0.5\sigma_0$.
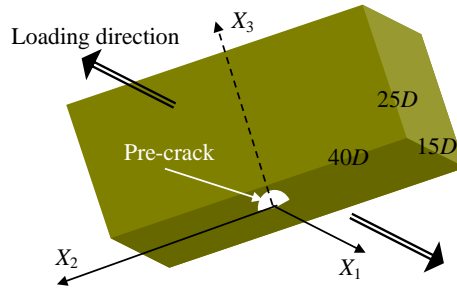

Figure 5. Schematic of 3D geometry (the solid region is tessellated into assembly of mecons)

For comparing finite element results with theory, the theoretical value of the stress intensity factor for semi-elliptic surface crack is used [23]. Fig. 6 illustrates a semi-elliptic crack, where the crack size in the X_3 direction is assumed to be the larger semi-axis.
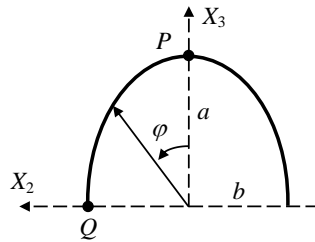

Figure 6. Semi-elliptic surface crack for theoretical computation of stress intensity factors

The stress intensity factor is a function of the position along the crack front, given by an angle φ measured from the larger semi-axis a, and depends on the remote load, given by σ_∞, and the sizes of the two semi-axes a and b ($a > b$). The expression reads

$$K_I = \frac{\sigma_\infty \sqrt{\pi b}}{E(m)} (1 - m^2 \cos^2 \varphi)^{1/4}, \tag{1}$$

where m is the axes mismatch parameter given by

$$m = \sqrt{1 - \frac{b^2}{a^2}}, \tag{2}$$

and $E(m)$ is the complete elliptic integral of the second kind, defined as

$$E(m) = \int_0^{\pi/2} \sqrt{1 - m^2 \sin^2 \theta} \, d\theta. \tag{3}$$

To account for the finite geometry considered in Fig. 5, correction factors have been applied to the value obtained by (1). These correction factors have been taken from 2D solutions that can be found in [23]. The correction factor for determining the stress intensity factor at point P in Fig. 6 is the one used for an edge crack of size a in a finite plate of thickness $W = 25D$ (see Fig. 5) and is given in terms of the parameter $\alpha = a / W$ with

$$F_3(\alpha) = 1.12 - 0.231\alpha + 10.55\alpha^2 - 21.72\alpha^3 + 30.39\alpha^4. \tag{4}$$

Eq. (4) gives an error of ±0.5% for $\alpha \leq 0.6$. The correction factor for determining the stress intensity factor at point Q in Fig. 6 is the one used for a central crack of size $2b$ in a finite plate of thickness $W = 40D$ (see Fig. 5) and is given in terms of $\alpha = 2b / W$ with

$$F_2(\alpha) = \left(1 - 0.025\alpha^2 + 0.06\alpha^4\right)\sqrt{\sec\left(\frac{\alpha\pi}{2}\right)}. \tag{5}$$

Eq. (5) gives an error of ±0.2% for any α. The finite geometry in the loading direction, X_1, has not been accounted for.

Computationally, two stress intensity factors considered as measures for the crack driving force have been determined in a standard (approximate) way via the stresses ahead of the crack front in X_2 and X_3 directions, respectively. An illustration of a developed crack in the X_2-X_3 plane is shown in Fig. 7 in green.
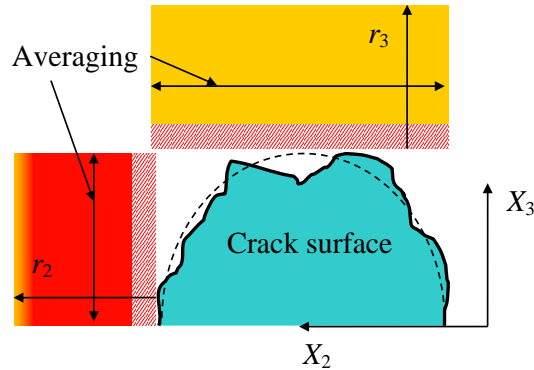

Figure 7. Illustration of numerical computation of stress intensity factors

The dotted line shows the corresponding semi-elliptic crack of the same semi-axes that have been used for comparisons. The rectangles ahead of the crack front in the two directions considered show the regions accounted for in determining the stress intensity factors. These rectangular regions are the projections onto the X_2-X_3 plane of parallelepipeds that extend in the X_1-direction over the real crack thickness, i.e. several grains corresponding to the current crack geometry out of plane. The estimated plastic zones are dashed (~one grain), while the rest of the rectangular regions are taken to span over five grains in the corresponding direction. Consider the calculation of the stress intensity factor in the X_3 – direction, which is to be compared to the value given by Eq. (1) at $\varphi = 0$ multiplied by the correction factor Eq. (4). The stress in the direction of load application, σ_{11}, (out of the plane of the figure) is the only one taken into account in calculating the stress intensity factor. For any given distance from the crack front, r_3, in steps of one grain diameter, a stress σ_{11} has been obtained by averaging the stresses in all grains with the corresponding X_3-coordinate along the line shown in the figure and in thickness of the parallelepiped in X_1-direction. Thus, an approximate relationship $\sigma_{11}(r_3)$ has been established. The function

$$\kappa\left(r_3\right) = \sigma_{11}\left(r_3\right)\sqrt{2\pi r_3} \,, \tag{6}$$

possesses nearly linear behaviour in the considered range of r_3 and by extrapolating this linear relationship to $r_3 = 0$, the stress intensity factor at the crack front is found, i.e.

$$\sigma_{11}\left(r_3\right)\sqrt{2\pi r_3} \xrightarrow{r_3 \to 0} K_I^{FEM} \,. \tag{7}$$

The stress intensity factor in the X_2 – direction is calculated in an identical way and is to be compared to the value given by Eq. (1) at $\varphi = \pi / 2$ multiplied by the correction factor Eq. (5). It should be noted, that the stress intensity factors thus determined are not used in the criterion for grain boundary failure. Failures are decided solely on the basis of local strain fields, found with finite element calculations.

A post-processing computer programme has been developed to implement the computational procedure described above for determining the stress intensity factors. The programme takes the finite element results after each step of the simulations and delivers the required stress intensity factors, as well as the current crack geometry including the number of bridges along the crack surface. The bridges can be in elastic regime or yielding. In addition, the programme calculates the shielding effect of the bridges (total and that due only to yielding bridges) via the stress intensity factor that the bridges create with respect to the corresponding crack fronts. The stress intensity due to all bridges is an algebraic sum of the contributions from every bridge, given by the formula:

$$K_{br} = F_i\left(\alpha\right) P \sqrt{\frac{\pi}{2r}} \,, \tag{8}$$

where P is the force in the bridge parallel to the loading (crack opening) direction, r is the distance to the corresponding crack front and $F_i(\alpha)$ is given by either Eq. (4) for stress intensity sought in the X_3 – direction or by Eq. (5) for stress intensity sought in X_2 direction. Eq. (8) is the solution for a crack loaded in Mode I by a couple of symmetric concentrated forces of magnitude P placed on the crack surfaces at distance r from the tip [23]. The programme has been checked with developed cracks of nearly semi-elliptic shape with no bridges to compare with theoretical values given by Eq. (1) in combination with Eq. (4) or Eq. (5). These checks have been performed for a range of crack sizes from one grain to eight

grains in depth. Results of the computational and theoretical approaches are almost identical, with an error of less than 0.01%, which gives confidence in the stress intensity factors procedure as well as in the mechanical model adopted.

3.2. 2D GEOMETRY PROBLEMS

The 2D geometry is considered because it allows for significantly larger assemblies to be modelled and solved in a reasonable time. All the problems studied share the same geometry. With respect to a fixed coordinate system (X_1, X_2), the assembly of grains fills the rectangular region $\{-50D \leq X_1 \leq 50D, 0 \leq X_2 \leq 50D\}$. This region contains 7740 grains, which form 22850 internal grain boundaries, modelled by 7740 nodes and 22850 beam elements in the finite element model. The load is symmetric and applied via prescribed displacements: $u_1 = -0.025D$ along the boundary $\{X_1 = -50D, 0 \leq X_2 \leq 50D\}$ and $u_1 = 0.025D$ along the boundary $\{X_1 = 50D, 0 \leq X_2 \leq 50D\}$. Displacements $u_2 = 0$ are prescribed along the boundary $\{-50D \leq X_1 \leq 50D, X_2 = 50D\}$, while zero stresses are prescribed for all other boundary conditions. As for 3D problems, these conditions introduce a homogeneous strain in the assembly $\varepsilon_\infty = 5 \times 10^{-4}$, equivalent to a homogeneous stress $\sigma_\infty \approx 0.5\sigma_0$.

An initial crack, extending along three grain boundaries, is introduced from the surface point at the origin of the coordinate system and running in towards the centre of the element assembly. As for 3D problems, the analytical value of the stress intensity factor is used for comparative purposes. In this case, the value for a straight edge crack in a finite geometry has been used [23]

$$K_I = F_3(\alpha)\sigma_\infty\sqrt{\pi a}, \tag{9}$$

where a is the crack extension, σ_∞ is the remote load and $F_3(\alpha)$ is given by Eq. (4) for parameter $\alpha = a / W$ with $W = 50D$.

Computationally, the stress intensity factor is calculated in a way similar to the one described for 3D problems. An illustration is given in Fig. 8, where a portion of the solid is shown. The actual crack is given with a thick white line and a possible bridge along the crack path is depicted with a green one. The corresponding straight crack for theoretical calculations is also shown. The rectangle ahead of the crack tip shows the region accounted for in determining the stress intensity factors. The possible plastic zone is dashed with red lines, while the rest of the rectangular region is taken to span over ten grains.
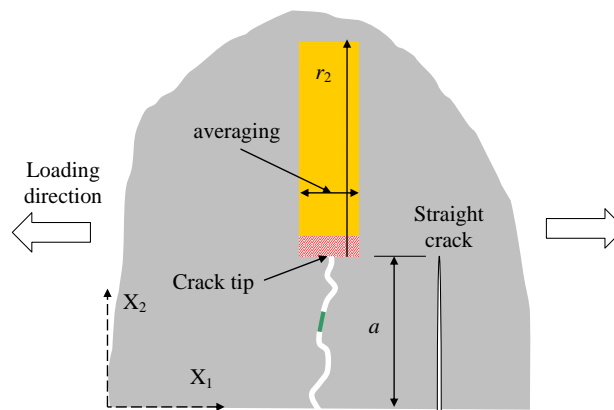

Figure 8. Numerical calculation of stress intensity factor in 2D

Again, for any given distance from the crack tip, r_2, with a step one grain diameter, a stress σ_{11} has been calculated by averaging the stresses in all grains along the line shown in the figure. The approximate relationship $\sigma_{11}(r_2)$ established is used to calculate the stress intensity factor via Eq. (7) replacing r_3 with r_2.

Similarly to the 3D problems, a post-processing computer programme has been developed to implement the computational procedure for determining the stress intensity factors. It delivers the stress intensity factor and the current crack geometry including the number of bridges along the crack surface after each step of the simulations. Determination of the bridges shielding effect is done in a manner identical to the 3D model via the stress intensity factors from all bridges calculated using Eq. (8) with $F_i(\alpha)$ given by Eq. (4). This programme has been checked with developed straight cracks without bridges or branches (zig-zag cracks in the hexagonal microstructure) for the entire range of crack extensions between one grain and 25 grains. Comparison with theoretical values given by Eq. (9) and Eq. (4) showed identical results for the stress intensity factors.

LITERATURE

1. *Gourgues, A. -F.* Electron backscatter diffraction and cracking. Mater. Sci. Tech. 18: 119–133, 2002.

2. *Pfaendtner, J. A., R. C. Muthiah, C. T. Liu, C. J. McMahon.* Time-dependent interfacial failure of metallic alloys. Mater. Sci. Eng. A 260: 1–11, 1999.

3. *Scully, J. R.* Environment-assisted intergranular cracking. MRS Bulletin 24: 36–42, 1999.

4. *Randle, V.* Crystallographic characterization of planes in the scanning electron-microscope materials characterization. Mater. Characterization 34: 29–34, 1995.

5. *Lin, P., G. Palumbo, U. Erb, K. T. Aus.* Influence of grain-boundary-character-distribution on sensitization and intergranular corrosion of alloy-600. Scripta Metall. Mater. 33: 1387–1392, 1995.

6. *Pan, Y., B. L. Adams, T. Olson, N. Panayotou.* Grain-boundary structure effects on intergranular stress corrosion cracking of alloy X-750. Acta Mater. 44: 4685-4695, 1996.

7. *Bruemmer, S. M., G. S. Was.* Microstructural and microchemical mechanisms controlling intergranular stress corrosion cracking in light-water-reactor systems. J. Nuclear Mater. 216: 348–363, 1994.

8. *Gertsman, V. Y., S. M. Bruemmer.* Study of grain boundary character along intergranular stress corrosion crack paths in austenitic alloys. Acta Mater. 49: 1589–1598, 2001.

9. *Watanabe T., S. Tsurekawa.* The control of brittleness and development of desirable mechanical properties in polycrystalline systems by grain boundary engineering. Acta Mater. 47: 4171–4185, 1999.

10. *Lehockey, E. M., G. Palumbo, P. Lin, A. M. Brennenstuhl*. On the relationship between grain boundary character distribution and intergranular corrosion. Scripta Mater. 36: 1211–1218, 1997.

11. *Palumbo, G., P. J. King, K. T. Aust, U. Erb, P. C. Lichtenberger.* Grain-boundary design and control for intergranular stress-corrosion resistance. Scripta Metall. Mater. 25: 1775–1780, 1991.

12. *Lehockey, E. M., A. M. Brennenstuhl, I. Thompson*. On the relationship between grain boundary connectivity, coincident site lattice boundaries, and intergranular stress corrosion cracking. Corros. Sci. 46: 2383–2404, 2004.

13. *Gertsman, V. Y., K. Tangri*. Modelling of intergranular damage propagation. Acta Mater. 45: 4107–4116, 1997.

14. *Lim, L. C., T. Watanabe.* Fracture-toughness and brittle-ductile transition controlled by grain-boundary character distribution (GBCD) in polycrystals. Acta Metall. Mater. 38: 2507–2516, 1990.

15. *Frary, M., C. A. Schuh.* Connectivity and percolation behaviour of grain boundary networks in three dimensions. Philos. Mag. 85: 1123-1143, 2005.

16. *Marrow, T. J., L. Babout, A. P. Jivkov, P. Wood, D. Engelberg, N. Stevens, P. J. Withers, R. C. Newman*. Three dimensional observations and modelling of intergranular stress corrosion cracking in austenitic stainless steel. J. Nucl. Mater. 352: 62–74, 2006.

17. *Babout, L., T. J. Marrow, D. Engelberg, P. J. Withers.* X-ray microtomographic observation of intergranular stress corrosion cracking in sensitised austenitic stainless steel. Mater. Sci. Techn. 22: 1068–1075, 2006.

18. *Jivkov, A. P., N. P. C. Stevens, T. J. Marrow*. A 2D mesoscale model for intergranular stress corrosion crack propagation. Acta Mater. 54: 3493–3501, 2006.

19. *Jivkov, A. P., N. P. C. Stevens, T. J. Marrow*. A three-dimensional computational model for intergranular cracking. Comput. Mater. Sci. 38: 442–453, 2006.

20. *Jivkov, A. P., N. P. C. Stevens, T. J. Marrow*. Modelling intergranular stress corrosion cracking in simulated three-dimensional microstructures. Submitted to Key Eng. Mater.

21. *Thomas, L. E., S. M. Bruemmer*. High-resolution characterization of intergranular attack and stress corrosion cracking of Alloy 600 in high-temperature primary water. Corrosion 56: 572–587, 2000.

22. ABAQUS User's Manual, Version 6.5, Abaqus Inc., 2005.

23. *Tada, H., P. C. Paris, G. R. Irwin*. The stress analysis of cracks handbook, 3d Ed. ASME Pres: New York, 2000.

Submitted: March 2007

МОДЕЛИРАНЕ НА МЕЖДУЗЪРНЕСТ РАСТЕЖ НА ПУКНАТИНИ В ПОМОЩ НА МИКРОСТРУКТУРНОТО ИНЖЕНЕРСТВО. ЧАСТ I: МОДЕЛИ

А. Живков[1]

РЕЗЮМЕ

В тази първа част на труда е представено подробно описание на нов равнинен и нов пространствен модел за изучаване на междузърнесто, подпомогнато от околната среда напукване при поликристални материали. Тези модели са разработени, за да се отстранят ограниченията на перколационните модели, ползвани преди за оценка на съпротивата на материала срещу междузърнесто напукване. Перколационните модели не отчитат механичната движеща сила за растеж на пукнатината, което ограничава тяхното приложение. Новите модели се базират на регулярно дискретно представяне на микроструктурата на материала и на бинарен избор на междузърнестите граници, където те са приети да бъдат или податливи, или устойчиви на междузърнесто напукване в зависимост от тяхната кристалографска характеристика. Описани са още решените проблеми и методите за анализ на резултатите, представени във втората част на труда.

---

[1] Андрей Живков, The University of Manchester, School of Materials, Grosvenor Street, Manchester M1 7HS, UK; Tel: +44 (0)161 3063556; Fax: +44 (0)161 3063586; E-mail: andrey.jivkov@manchester.ac.uk